Impedance-based Root Cause Analysis and Grid-Side Damping of a Converter Driven Low-Frequency Oscillation in a High-IBR Grid

Sungjun Kim and Kyeon Hur
School of Electrical and Electronic Engineering
Yonsei University
Seoul, South Korea
{sjkim95, khur}@yonsei.ac.kr

Chongho Rhim and Seokju Kang
General manager and Senior Researcher
Korea Electric Power Corporation(KEPCO)
Naju, South Korea
{chongho.rhim, sj_kang}@kepco.co.kr

***Abstract*—Power systems with high penetration of inverter-based resources and limited synchronous support can exhibit low-frequency oscillations driven by power electronic converters rather than by synchronous machine modes. This paper presents a framework to diagnose and mitigate such oscillations in an inverter-dominated grid. First, small-signal impedance scans at converter points of common coupling are used to obtain dq-frame admittance, identify a weakly damped mode, and link it to a specific converter interaction. The mode's impact is confirmed in a large-scale electromagnetic transient simulation of a credible scenario in which the loss of a remaining synchronous generator produces an oscillation such that the system does not settle to a new operating point. Finally, grid-side damping control is applied through existing STATCOM, and the same contingency settles to a stable operating point. The proposed framework enables practical root-cause analysis and mitigation even when detailed vendor control models are not available.**

***Index Terms*—Electromagnetic transient simulation, impedance analysis, inverter-based resources, low-frequency oscillations, small-signal stability.**

I. Introduction

High penetration of IBRs such as high-voltage direct current (HVDC) links, renewable energy sources, and grid-support converters is fundamentally changing the dynamic behavior of bulk power systems [1]–[4]. As synchronous machines are displaced or operated closer to its limits, system stability is no longer governed solely by electromechanical swing dynamics [1], [4]. Instead, the multi-loop control structure of converters can strongly influence the system response [5]–[8]. These mechanisms are not explicitly resolved in conventional phasor-domain simulation tools such as PSS®E, where converter controls are typically represented in an aggregated or simplified form rather than modeled in full detail [9]. As a result, under large disturbance conditions, instability can be driven primarily by converter behavior rather than by classical synchronous machine modes [3].

This study is the result of a research project conducted with the funds of the Open R&D(R24TO01) Program of Korea Electric Power Corporation. Also, this research was in part supported by the NRF grant funded by the MSIT (No. 2021R1A2C209550313, RS-2023-00218377).(*Corresponding Author: Kyeon Hur.*)

Recent events in grids with high penetration of IBRs have shown that, after a severe disturbance, the system can exhibit a persistent low-frequency oscillation that does not match traditional inter-area or local modes [3]. To investigate such events, two main analysis approaches are widely used. One approach performs impedance scanning at converter terminals to characterize resonant modes and weakly damped frequency ranges, even when only black-box models are available [5]–[7]. A second approach linearizes the system and performs small-signal analysis to identify poorly damped oscillatory modes [10]. These studies show that converter-driven oscillations can arise in weak grids [3], [4], [8], and most prior work has focused on resonance at the level of a single IBR or a simplified test system. However, they typically emphasize general grid weakness rather than identifying which specific converter and mode lose damping after a given contingency, and they rarely extend to large interconnected networks [8]. In addition, mitigation is often framed as retuning the affected IBR's internal control parameters, which may not be practical for system operators, rather than as providing external damping support that can be deployed at the system level.

This paper proposes a stability assessment and mitigation framework that combines impedance analysis of black-box converters and the network with large-scale EMT simulation. The framework first uses operating point dependent impedance analysis of black-box converters to identify the converter-driven oscillatory mode. It then verifies in a large-scale EMT model that this mode can drive unstable operations, and finally demonstrates grid-side damping control can suppress the oscillation without relying on detailed knowledge of the converter's internal controls.

II. Impedance Based Diagnosis And Mitigation Framework

Figure 1 summarizes the framework used in this paper to assess and mitigate converter-driven stability risks in IBR-rich power systems. It addresses cases where system conditions (e.g., network contingencies, network strength, dispatch and control settings) allow converter–grid interactions to excite

979-8-3315-8138-1

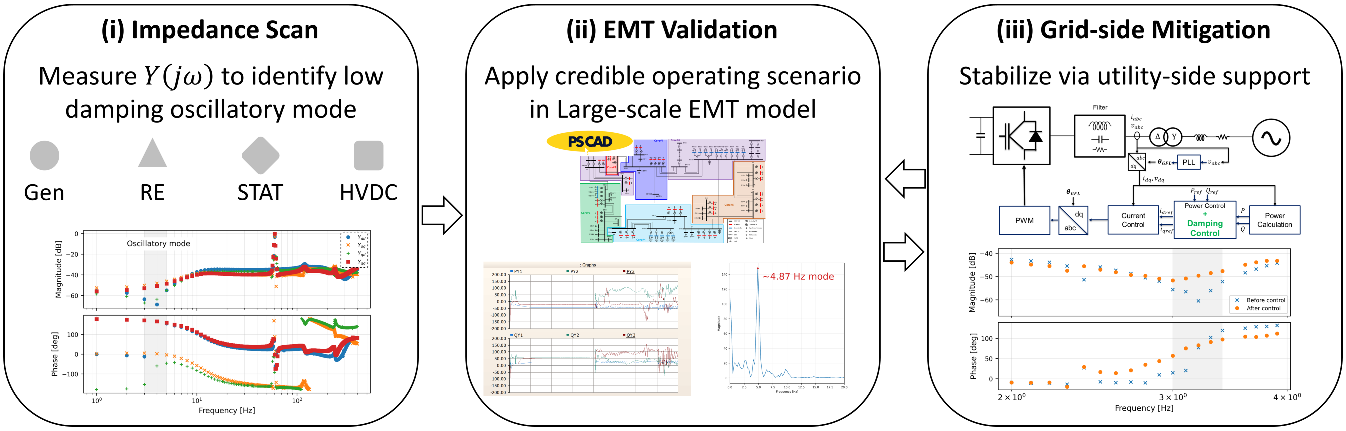

Fig. 1. Impedance-based diagnosis and mitigation workflow.

lightly damped oscillatory modes that may threaten system stability. The process has three stages: (i) operating point dependent impedance scanning at selected converter interfaces to identify low-damping modes; (ii) large-scale EMT verification to determine whether the identified mode governs the time-domain response; and (iii) grid-side damping provision (e.g., damping control added to existing converter or deployment of grid-forming control), followed by time-domain simulation confirmation. Sections II-A through II-C detail each stage.

A. Impedance Based Identification of a Weakly Damped Oscillatory Mode

Stage (i) characterizes the local small-signal behavior at converter/grid point of common coupling (PCC) using an impedance (or admittance) scan. Small sinusoidal perturbations are injected on the d- and q-axis voltage references at the PCC, one axis and one frequency at a time, and the resulting d-q current response is recorded. Sweeping across frequency in this way yields the local admittance matrix

$$\mathbf{Y}(j\omega) = \begin{bmatrix} Y_{\mathrm{dd}}(j\omega) & Y_{\mathrm{dq}}(j\omega) \\ Y_{\mathrm{qd}}(j\omega) & Y_{\mathrm{qq}}(j\omega) \end{bmatrix}, \tag{1}$$

where, for example, $Y_{\mathrm{dd}}(j\omega) = \Delta I_{\mathrm{d}}/\Delta V_{\mathrm{d}}$ and $Y_{\mathrm{dq}}(j\omega) = \Delta I_{\mathrm{d}}/\Delta V_{\mathrm{q}}$. Here ΔV_{d} and ΔV_{q} are small injected test voltages in the synchronous reference frame, and $\Delta I_{\mathrm{d}}, \Delta I_{\mathrm{q}}$ are the measured current responses at that same PCC.

The corresponding impedance matrix

$$\mathbf{Z}(j\omega) = \mathbf{Y}(j\omega)^{-1} \tag{2}$$

can be formed when an impedance view is more convenient. In practice, the scan is applied to both sides of the interface: (i) the machine-side terminal admittance/impedance of a black-box converter (HVDC, STATCOM, etc.), and (ii) the grid-side admittance/impedance as seen from the same PCC into the surrounding network. A lightly damped oscillatory mode appears as a narrow, pronounced feature in magnitude with a rapid phase change over a small frequency band, whereas well-damped dynamics produce flatter magnitude and smoother phase variation.

Because scans are performed at a specific steady-state operating point, the obtained $\mathbf{Y}(j\omega)$ and $\mathbf{Z}(j\omega)$ depend on the dispatch, converter set points, and network topology. Repeating the scan under alternative operating conditions makes shifts in resonant frequency and changes in apparent damping explicit. Operating points that produce a sharp resonance with limited apparent damping are identified as high-risk scenarios. Importantly, the procedure relies only on terminal perturbations and PCC measurements; no access to internal controller models is required, which makes the procedure suitable for large networks with vendor black-box models. However, exhaustive impedance scans over all system operating points are impractical, and this paper focuses on the operating condition under study.

B. EMT Validation Under a Credible Scenario

Stage (ii) evaluates, in a large-scale EMT model of the network, whether the operating condition flagged in Stage (i) can in fact lead to unstable post-disturbance behavior. A representative disturbance is applied in the EMT model for that operating condition, and the resulting time-domain response is examined. The EMT model explicitly represents fast converter control loops and their interaction with the grid, which are not fully captured in reduced phasor-domain studies.

The objective is to determine whether the system converges to a bounded steady operating condition after the disturbance, or instead remains dominated by the oscillatory mode identified in Stage (i). If the system fails to converge and is driven by that mode, the scenario is classified as a system-level stability risk for that operating condition.

C. Grid-Side Damping Control

Stage (iii) moves from assessment to stabilization. Rather than retuning the internal controller of the converter involved in the weakly damped mode, damping is injected from the grid side using an existing grid-side resource (e.g., STATCOM, SVC, BESS inverter), subject to ownership/operational agreements. The objective is to counteract the identified mode without modifying the original converter's inner-loop parameters. Practically, an auxiliary supplementary damping control can be added to the selected resource [11] (or to a synchronous machine via a supplemental stabilizing loop). A compensator provides phase advance and gain in the narrow band around

979-8-3315-8138-1

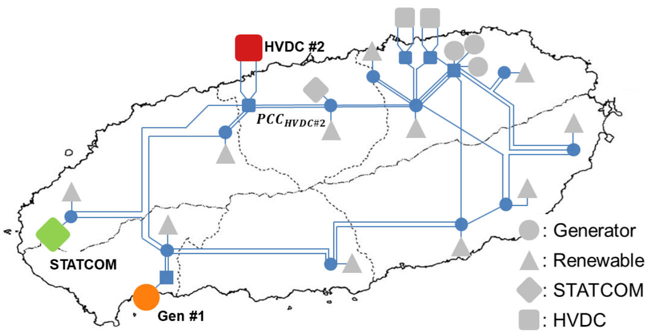

Fig. 2. Simplified single-line diagram of the Jeju grid, showing major inverter-based resources and synchronous generators.

TABLE I
OPERATING CONDITIONS FOR THE STUDIED SCENARIO IN THE JEJU GRID

Resource type	Flow [MW]	Capacity [MVA]
System demand (load)	1,189	–
Synchronous generators (total)	168	317
Gen #1	65	130
Renewable IBRs (PV + wind)	1,043	1,423
HVDC #1	-40	300
HVDC #2	40	400
HVDC #3	-22	200
STATCOMs (2 units)	–	50 (each)

the mode frequency and drives an external support command. Conceptually,

$$u^*(s) = K_{\text{damp}}\, H(s)\, \tilde{x}(s), \tag{3}$$

where $\tilde{x}(s)$ is the oscillatory component of a locally available signal (e.g., bus-voltage or frequency), $H(s)$ supplies the required phase compensation and band-limited gain, and $u^*(s)$ is the commanded support (such as a reactive current reference). By opposing the mode's phase, this loop increases effective damping from the grid side.

A complementary option is to operate a converter in grid-forming mode, which tightly regulates voltage magnitude and frequency [12] through droop and virtual-impedance mechanisms. With this control mode, the converter behaves as a stiff voltage source in the relevant band and can provide system-wide damping and stiffness without retuning other converters.

In this paper, the grid-forming implementation retains the same steady-state voltage reference and current/VAR limits as the original STATCOM; therefore, the pre-disturbance power-flow operating point is unchanged, while the modified dynamics provide additional damping in the oscillatory band.

To validate the mitigation, the same disturbance used in Stage (ii) is reapplied in the large-scale EMT model with the damping support enabled. Successful mitigation is confirmed when the previously dominant low-frequency mode no longer governs the post-disturbance response and the system converges to a bounded operating condition.

III. Case Study : Korea Jeju Grid

A large-scale EMT model of the Jeju grid is used to study a future, IBR-rich operating scenario. The network comprises three HVDC links, two STATCOMs, aggregated PV/wind plants, and a small set of synchronous generators; the HVDCs are represented by vendor-supplied black-box EMT models. Most active power is supplied by renewables, with only four synchronous units online. Additional transfer is provided through the HVDC links. Table I summarizes the operating point.

Fig. 2 locates the key interfaces on the single-line diagram: HVDC #2 (red square) is the converter interface where a low-frequency resonance is observed in the dq-frame admittance; Gen #1 (orange circle) is a tripped machine in this scenario and materially affects damping of that mode; and the selected STATCOM (green diamond) provides grid-side damping support. To compensate for the diminished damping contribution, the STATCOM located in the vicinity of Gen #1 was utilized. Its electrical proximity within the integrated Jeju grid ensures effective coupling to stabilize the dynamic response at the HVDC #2 PCC. All other resources are shown in gray for context. Impedance scans were performed at several PCCs (each HVDC terminal, renewables, and key synchronous generator buses) to compare machine-side and grid-side characteristics. For the 4.87 Hz case discussed here, the analysis is primarily referenced to the HVDC #2 terminal PCC, with complementary admittance scans at generator buses used to demonstrate the re-emergence of the resonance following Gen #1 trip. The remainder of this section follows the workflow in Fig. 1: Section III-A reports the impedance findings and flags the high-risk scenario; Section III-B verifies the resulting instability in time-domain EMT simulation; Section III-C demonstrates stabilization using grid-side damping control.

A. Impedance Based Mode Extraction and Attribution

The dq-frame admittance scan at the HVDC #2 terminals in Fig. 3(a) shows a characteristic low-frequency resonance under the steady-state operating point. A narrow feature appears around 3 Hz, indicating an oscillatory mode associated with the converter interface. Fig. 3(b) then examines the network admittance seen from the Gen #1 to illustrate how synchronous generator affects the apparent damping of this low-frequency resonance. With Gen #1 online ($Y_{\text{gen}} + Y_{\text{grid}}$: orange), the resonance is effectively suppressed: the magnitude trace around 3 Hz no longer exhibits a distinct peak and the phase is consistent with stabilizing damping contribution from the generator. When Gen #1 is out of service (Y_{grid}: blue), the same mode re-emerges as a clear low-damping resonance. Using a standard peak-picking estimate on the magnitude/phase around the peak, the damping ratio of this mode is approximately 1.56 %.

Fig. 4 examines how this mode depends on the HVDC #2 active power dispatch. As the converter's active power transfer increases, the dominant low-frequency resonance shifts to a higher frequency. In the post-contingency operating condition expected for the studied scenario, HVDC #2 is dispatched near 90 MW. Accordingly, the impedance scan predicts a dominant oscillation in the 4.8-5 Hz range. This attribution step therefore links the weakly damped mode to the HVDC #2 interface

979-8-3315-8138-1

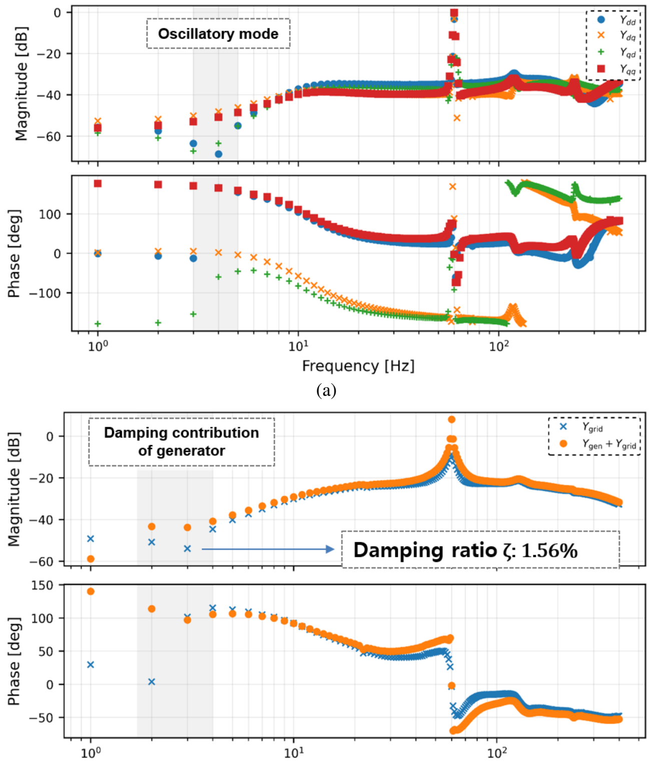

Fig. 3. Impedance characteristics. (a) dq-frame admittance of HVDC #2. (b) Whole-system admittance with resonance shift and damping loss after synchronous generator outage.

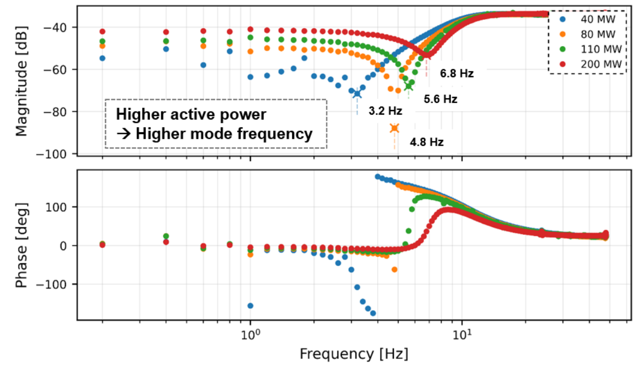

Fig. 4. Operating point dependence of the critical oscillatory mode associated with HVDC #2.

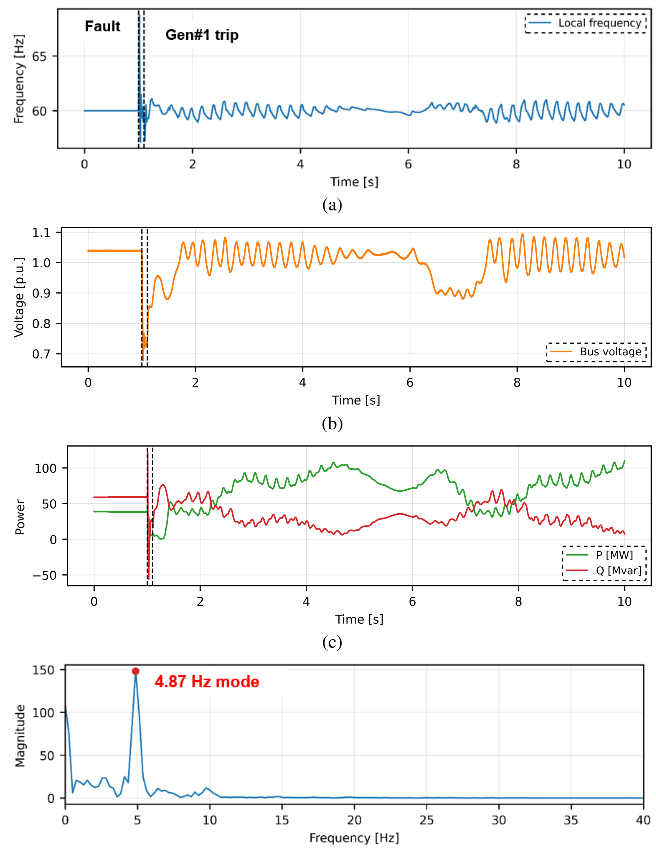

Fig. 5. EMT simulation of the generator trip contingency. (a) System frequency. (b) Bus voltage. (c) HVDC #2 power. (d) FFT of bus voltage.

and quantifies how its frequency varies with the converter's operating point, while highlighting the stabilizing contribution that Gen #1 provides when in service.

B. Post-Contingency Low-Frequency Oscillation

The scenario inferred in Section III-A is now exercised in the full large-scale EMT model of the Jeju grid. A local three-phase fault is applied near Gen #1 at $t = 1.0$ s and cleared by tripping Gen #1 at $t = 1.1$ s. This creates an operating condition in which HVDC #2 must supply the lost active power that had been provided by the synchronous generator, while the local damping contribution of Gen #1 is no longer available.

The resulting time-domain response is shown in Fig. 5. Immediately after the trip, HVDC #2 increases its active power injection to replace the lost generation and the area frequency and bus voltage exhibit a low-frequency oscillation. The FFT analysis of the bus-voltage waveform reveals a clear peak around 4.87 Hz, consistent with the resonance predicted by the impedance assessment in Fig. 4.

This confirms that the instability mechanism is not a classical inter-area or local synchronous machine swing mode, but a converter-associated mode that becomes insufficiently damped once Gen #1 is removed and HVDC #2 is dispatched to a higher active power output.

C. Grid-Side Damping Control

To determine whether the instability identified in Section III-B can be eliminated without modifying the internal controller of HVDC #2, grid-side damping support was introduced using converters already present in the system. Two complementary approaches were evaluated as shown in Fig. 6.

1) STATCOM with narrow-band damping: The existing STATCOM was augmented with a narrow-band lead–lag compensator tuned around the identified mode (≈4.8 Hz). The compensator uses the local PLL frequency as an input and shapes a small damping signal that is summed into the STATCOM i_q reference.

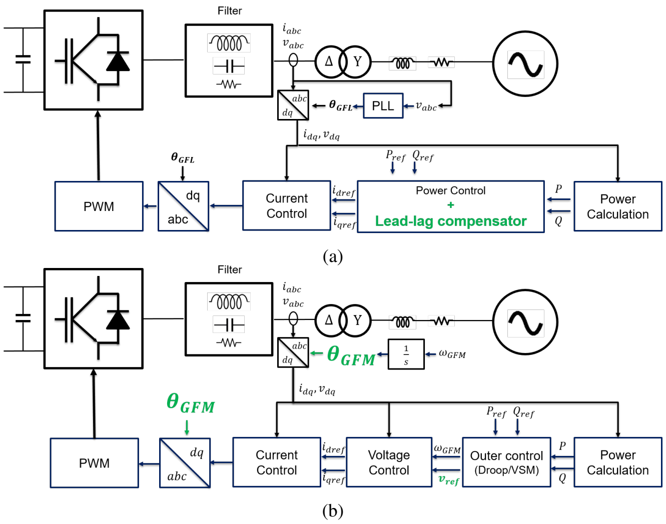

Fig. 6. STATCOM with damping control. (a) Lead-lag compensator. (b) Grid-forming control.

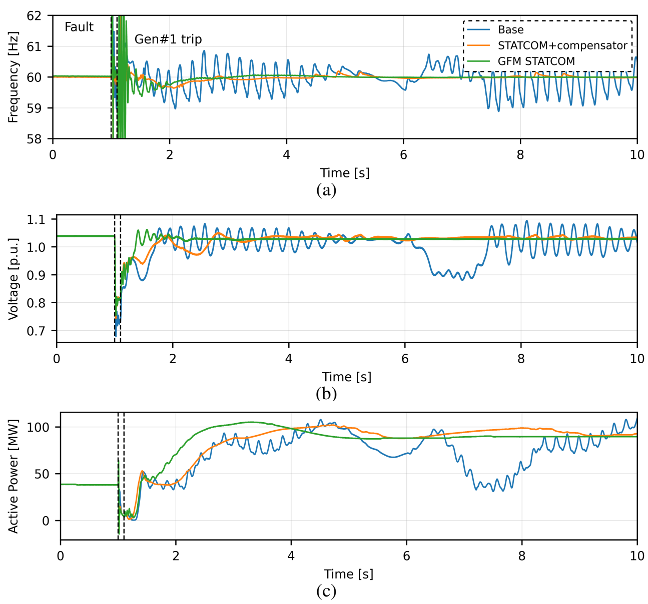

Fig. 7. Effect of grid-side damping control. (a) System frequency. (b) Bus voltage. (c) HVDC #2 active power.

2) STATCOM with Grid-forming control: As a control architectural mitigation, a converter was operated in a grid-forming mode to provide stiff voltage regulation and inertial like damping near the oscillatory band. In this configuration the interface behaves as an active stabilizing source for the local bus rather than a purely grid-following converter.

The same disturbance of Section III-B was then reapplied with each mitigation enabled. Fig. 7 compares the post-disturbance responses. In both cases the 4.87 Hz oscillation is suppressed: the system frequency and bus voltage converge to bounded steady trajectories, and HVDC #2 active power settles without sustained oscillation. These results demonstrate that stabilization can be achieved at the grid-side, using operator-accessible converter, without retuning or exposing the detailed internal controls of HVDC #2.

IV. Conclusion

This paper presented a stability assessment and mitigation approach for a high penetration IBR grid using an EMT model of the Jeju system. Impedance-based analysis showed that a converter-driven low-frequency oscillatory mode is normally suppressed when Gen #1 is online, but reappears with low damping ratio 1.56 % when generator is lost and its active power must be supplied by HVDC #2. When this loss of Gen #1 contingency was applied in EMT simulation, the system failed to settle to a new steady operating point and instead remained dominated by that converter-driven low-frequency oscillatory mode, confirming that the instability mechanism is not a classical synchronous machine swing mode. The same contingency was then stabilized by adding grid-side damping support through an existing STATCOM, without retuning or exposing the internal control parameters of the HVDC converter. These results indicate that such low-frequency oscillatory modes can become the limiting stability mechanism in high-IBR operating conditions, and that they can be identified, reproduced, and mitigated through a practical workflow that combines impedance analysis with large-scale EMT simulation.

References

[1] N. Hatziargyriou, J. Milanovic, C. Rahmann, V. Ajjarapu, C. Canizares, I. Erlich, D. Hill, I. Hiskens, I. Kamwa, B. Pal, P. Pourbeik, J. Sanchez-Gasca, A. Stankovic, T. Van Cutsem, V. Vittal, and C. Vournas, "Definition and classification of power system stability – revisited extended," *IEEE Transactions on Power Systems*, vol. 36, no. 4, pp. 3271–3281, 2021.

[2] L. Shen, M. Barnes, R. Preece, J. V. Milanovic, K. Bell, and M. Belivanis, "The effect of vsc-hvdc control on ac system electromechanical oscillations and dc system dynamics," *IEEE Transactions on Power Delivery*, vol. 31, no. 3, pp. 1085–1095, 2016.

[3] G. Wu, H. Sun, B. Zhao, S. Xu, X. Zhang, A. Egea-Àlvarez, S. Wang, G. Li, Y. Li, and X. Zhou, "Low-frequency converter-driven oscillations in weak grids: Explanation and damping improvement," *IEEE Transactions on Power Systems*, vol. 36, no. 6, pp. 5944–5947, 2021.

[4] U. Markovic, O. Stanojev, E. Vrettos, P. Aristidou, and G. Hug, "Understanding stability of low-inertia systems," 2019.

[5] J. Sun, "Impedance-based stability criterion for grid-connected inverters," *IEEE Transactions on Power Electronics*, vol. 26, no. 11, pp. 3075–3078, 2011.

[6] M. Cespedes and J. Sun, "Impedance modeling and analysis of grid-connected voltage-source converters," *IEEE Transactions on Power Electronics*, vol. 29, no. 3, pp. 1254–1261, 2014.

[7] X. Wang, L. Harnefors, and F. Blaabjerg, "Unified impedance model of grid-connected voltage-source converters," *IEEE Transactions on Power Electronics*, vol. 33, no. 2, pp. 1775–1787, 2018.

[8] L. Huang, H. Xin, W. Dong, and F. Dörfler, "Impacts of grid structure on pll-synchronization stability of converter-integrated power systems," *IFAC-PapersOnLine*, vol. 55, no. 13, pp. 264–269, 2022.

[9] J. Mahseredjian, V. Dinavahi, and J. A. Martinez, "Simulation tools for electromagnetic transients in power systems: Overview and challenges," *IEEE Transactions on Power Delivery*, vol. 24, no. 3, pp. 1657–1669, 2009.

[10] L. Fan, Z. Miao, and Z. Wang, "A new type of weak grid ibr oscillations," *IEEE Transactions on Power Systems*, vol. 38, no. 1, pp. 988–991, 2023.

[11] R. Sadikovic, P. Korba, and G. Andersson, "Application of facts devices for damping of power system oscillations," in *2005 IEEE Russia Power Tech*, 2005, pp. 1–6.

[12] S. Shah, W. Yan, P. Koralewicz, V. Gevorgian, D. Ramasubramanian, R. Wallen, A. Hoke, B. Kroposki, and B. Mather, "A testing framework for grid-forming resources," in *2023 IEEE Power Energy Society General Meeting (PESGM)*, 2023, pp. 1–5.

979-8-3315-8138-1